

# Evaluating glioma growth predictions as a forward ranking problem

Karin A. van Garderen<sup>1</sup>, Sebastian R. van der Voort<sup>1</sup>, Maarten M.J. Wijnenga<sup>1</sup>, Fatih Incekara<sup>1,2</sup>, Georgios Kapsas<sup>1</sup>, Renske Gahrman<sup>1</sup>, Ahmad Alafandi<sup>1</sup>, Marion Smits<sup>1</sup>, and Stefan Klein<sup>1</sup>

<sup>1</sup> Department of Radiology and Nuclear Medicine, Erasmus MC, Rotterdam

<sup>2</sup> Department of Neurosurgery, Erasmus MC, Rotterdam

**Abstract.** The problem of tumor growth prediction is challenging, but promising results have been achieved with both model-driven and statistical methods. In this work, we present a framework for the evaluation of growth predictions that focuses on the spatial infiltration patterns, and specifically evaluating a prediction of future growth. We propose to frame the problem as a ranking problem rather than a segmentation problem. Using the average precision as a metric, we can evaluate the results with segmentations while using the full spatiotemporal prediction. Furthermore, by separating the model goodness-of-fit from future predictive performance, we show that in some cases, a better fit of model parameters does not guarantee a better the predictive power.

**Keywords:** Glioma · Growth model · Validation · Magnetic Resonance Imaging · Brain

## 1 Introduction

As the diagnosis and delineation of glioma has improved with machine learning [4], researchers look towards the more challenging task of predicting the disease trajectory into the future [19,8]. However, the problem of tumor growth is challenging in many ways, not just by the lack of publicly available data. The variables of clinical importance, such as the speed of infiltration and proliferation, are unknown and the problem of estimating them from observations is ill-posed. Furthermore, the observations we do have are flawed as tumor cells are known to spread beyond the visible boundary on MR imaging [22], which poses a challenge not just in prediction but also in validation of that prediction.

Despite these challenges, biophysical growth models have shown promise in their ability to predict the spatial growth patterns for individual cases. They are model-driven rather than data-driven, and strongly rooted in a mechanistic understanding of tumor growth. Delineations of the tumor on MR imaging typically form the input for individual model fitting, with follow-up imaging providing the gold standard of evaluation. Though other methods of evaluation exist, such as biopsy samples [10] or PET imaging [18], for most clinical cases consecutive delineations are the best approximation for a ground truth.

Due to the nature of the data, growth predictions are often framed as a segmentation problem. For example, by using an overlap metric such as the Dice Similarity Coefficient based on a sample in time [7,19]. Although this metric comes natural to the ground-truth data, it is less representative of the underlying problem. The main disadvantage of overlap-based metrics is that they treat all voxels equally, while some errors are more significant than others. Intuitively, we would want to assign more significance to false negative predictions at a large distance to the predicted tumor boundary as they are less in agreement to the model. This intuition is represented in metrics based on the segmentation boundary, such as the symmetric surface distance used in Konukoglu et al. [17]. But even a distance metric compares only to a single point in time, and using a boundary metric becomes less appropriate when the ground truth contains new disconnected lesions.

Another challenge in the evaluation of tumor growth predictions is the entanglement of model fit and prediction. All tumor growth models require an initial observation to fit model parameters. The segmentation on this initial observation serves as a measure for the goodness-of-fit and the prediction is performed from the time of onset, through the initial observation towards the future [3]. This work explores the distinction between goodness-of-fit and predictive performance by strictly separating them in the evaluation.

In this work we propose the following contributions:

1. A novel framing of tumor growth as a ranking problem, with the Average Precision as the performance metric
2. An experimental design that separates the prediction performance from the goodness-of-fit in both time and space
3. The application of this evaluation framework on a biophysical tumor growth model and a dataset of 21 patient cases, with low-grade glioma and partial tumor resection

## 2 Problem definition

### 2.1 Tumor growth as a ranking problem

To define the problem we must first define the shape of the expected solutions. We are interested in predicting infiltrative growth in a spatial sense. In other words, to simplify the problem we assume that the speed of growth and potential mass effect are not of interest. We assume that a growth model could produce a segmentation of the tumor  $S(t)$  at any time  $t > 0$ . It may therefore assign to every location in the brain a time  $T(x)$ , which is the first time  $t$  when the tumor reaches that location. As we do not require an accurate estimation of the growth speed, we require only that the estimated  $T(x)$  is a ranking of voxels in the brain, such that:

$$T(x_a) > T(x_b) \Leftrightarrow \exists t : x_a \notin S(t), x_b \in S(t). \quad (1)$$

The ranking can be evaluated by a sampling of the ground-truth segmentation  $S'$ , by using the Average Precision (AP). The AP is defined as the area under the Precision-Recall (PR) curve:

$$AP = \sum_t (R(t) - R(t-1))P(t), \quad (2)$$

where  $R(t)$  and  $P(t)$  are the recall and precision at a threshold  $t$  on the time-to-invasion ranking  $T$ , comparing to the segmentation  $S'$ . Since the precision scores are weighted by the difference in recall, all tumor volume predictions are taken into account from the tumor onset to the time when the recall is 1, meaning that the ground-truth segmentation is completely encompassed by the prediction. An evaluation based on a single time  $t$  would represent a point on the PR curve. If we take a volume-based sample, where the estimated tumor volume equals the observed tumor volume, this is the time  $t$  where  $R(t) = P(t)$ .

Formulating the problem as a ranking and using the AP has a number of qualitative advantages. First, the ranking  $T$  has a direct local connection to the speed of the tumor boundary. If the ranking is smooth, the gradient of the  $T$  represents the local movement of the visible tumor boundary. And yet, as a second advantage, the AP metric does not impose any assumption of smoothness on  $T$ . It automatically assigns a larger weight to certain parts of the prediction, depending on the assigned ranking  $T$ , regardless of any assumptions on the significance of distance in space or time. We might quantify the agreement between  $T$  and  $S$  locally by using the rank of the voxel  $T(x)$  as a threshold on the PR curve. A local prediction  $T(x)$  is in agreement with  $S$  if it is part of the reference segmentation ( $x \in S$ ) and can be included with high precision  $P(T(x))$ , or else if it falls outside  $S$  but can be excluded with high recall  $R(T(x))$ . Figure 1 illustrates the computation of the AP metric and this local measure of disagreement.

## 2.2 Experimental design

In the typical timeline of fit and evaluation [14,17], described in figure 2 as the bidirectional scheme, the model is fitted on a tumor segmentation  $S_0$  and then simulated from onset, through  $S_0$ , to the point of evaluation  $S_2$ . In other words, the prediction contains the behavior that it is fitted on.

We propose a strictly forward evaluation scheme that separates the model fit from the prediction as much as possible. As described in figure 2 as the forward scheme, the parameters are fitted on an initial time-point  $S_0$  and then used to make a prediction between two follow-up scans  $S_1$  and  $S_2$ . By running the prediction from a segmentation instead of an initial location, the need to fit the initial shape is removed and the evaluation is purely made on growth behavior that is unknown when fitting the model.

For our dataset, we need to consider the role of the tumor resection. In both schemes, the resection cavity as estimated by the alignment of the tissue at  $S_0$  and  $S_1$ , is removed from the region of interest for evaluation. In the forward scheme, any voxels in the segmentation  $S_1$  are also removed from the region

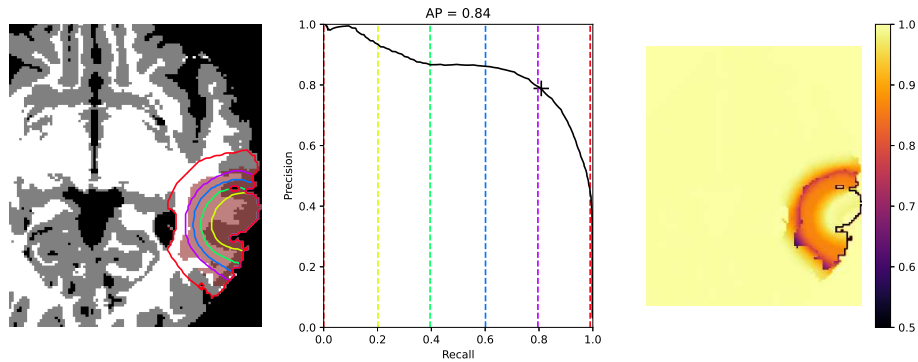


**Fig. 1.** Left: tissue segmentation of a specific case with thresholds on the  $T$  map, generated by a tumor growth model, indicated as segmentation boundaries. The ground-truth segmentation  $S$  is indicated by a red overlay. Middle: corresponding Precision-Recall curve with the same thresholds indicated. The sample with a corresponding volume is marked on the PR curve. Right: quantification of agreement by  $R(T(x))$  outside  $S$  and  $P(T(x))$  for voxels inside  $S$ .

of interest, leaving only the new growth visible in  $S_2$  for evaluation. So where the bidirectional scheme evaluates predictive performance on the entirety of the remaining tumor, using  $S_0$  only to initialize the location of onset, the forward scheme evaluates purely predictive performance based on the knowledge of  $S_1$ .

### 3 Methods

#### 3.1 Growth models

The model under evaluation is a traditional diffusion-proliferation model with anisotropic diffusion, informed by diffusion tensor imaging (DTI). The cell density  $c$  changes with each timestep  $dt$  according to:

$$\frac{dc}{dt} = \nabla(\mathbb{D}\nabla c) + \rho c(1 - c), \quad (3)$$

$$\mathbb{D}\nabla c \cdot n_{\delta\Omega} = 0, \quad (4)$$

where  $\rho$  is the growth factor,  $n_{\delta\Omega}$  is the normal vector at the brain boundary and  $\mathbb{D}$  is a tensor comprising an isotropic and anisotropic component:

$$\mathbb{D} = \kappa(x)\mathbb{I} + \tau F(x)\mathbb{T}(x), \quad (5)$$

where  $\kappa$  and  $\tau$  are parameters to weigh the two components,  $\mathbb{I}$  is the identity matrix,  $F(x)$  is the local Fractional Anisotropy (FA) and  $\mathbb{T}$  is the normalized diffusion tensor [11].

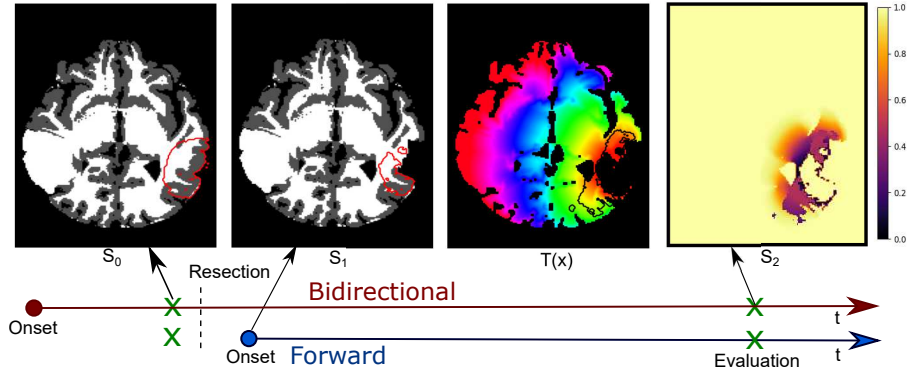


**Fig. 2.** Overview of two temporal evaluation schemes. Bidirectional: a growth model is fitted to the initial tumor and simulated from a seed point to generate a voxel ranking  $T$ . Forward: parameters are fitted to the initial tumor and then the model is initialized with a segmentation  $S_1$  obtained after resection to generate the voxel ranking  $T$ . Images from left to right: example of tissue segmentation with  $S_0$  outlined, tissue segmentation with resection cavity removed and  $S_1$  outlined, example of final ranking  $T$  used for the evaluation with resection cavity and  $S_1$  removed, quantification of agreement between  $T(x)$  and  $S_2$

The isotropic diffusion depends on the local tissue type [14], as defined by a separate parameter  $\kappa_w$  and  $\kappa_g$  for voxels in the white matter ( $\mathcal{W}$ ) and grey matter ( $\mathcal{G}$ ) respectively:

$$\kappa(x) = \begin{cases} \kappa_w & x \in \mathcal{W} \\ \kappa_g & x \in \mathcal{G} \end{cases}$$

To go from a prediction of  $c(t, x)$  to a time-to-invasion ranking  $T(x)$ , a threshold  $c_v$  is applied at each iteration such that  $T(x) = \min_t c(t, x) > c_v$ , where the visibility threshold is set as  $c_v = 0.5$ . The initial condition of the model is provided by an initial cell density  $c(t = 0)$ , which is a gaussian distribution centered at a location  $x_s$  and a standard deviation of 1mm. Alternatively, for the forward evaluation scheme, the model is initialized with a segmentation by setting the cell density at  $c = c_v$  for voxels inside the segmentation [7].

The model has four unknown parameters ( $\rho, \tau, \kappa_w, \kappa_g$ ) and an initial location  $x_s$ . It was implemented in Fenics [1] in a cubic mesh of 1mm isotropic cells, using a finite element approach and Crank-Nicolson approximations for the time stepping.

### 3.2 Eikonal approximation

The behavior of such a growth model can be approximated as a travelling wave, where the speed depends only on the local diffusion and proliferation properties.

Konokoglu et al. [17] have shown that such an eikonal approximation can effectively mimic the evolution of the visible tumor boundary. This approximation is especially useful for fitting the initial location  $x_s$  of a full growth model [21]. In this work, we use an eikonal approximation that assumes the visible tumor margin moves at a speed  $v$  of  $v = 4\sqrt{\rho \text{Tr}(\mathbb{D})}$ .

The eikonal approximation was used to estimate  $x_s$  for a given set of model parameters, by optimising the approximation of the initial tumor  $S_0$  using Powell’s method [20]. The best approximation was selected from multiple runs of the optimization with different random seeds.

### 3.3 Healthy brain structure

Running a growth model from onset requires knowledge of the underlying healthy tissue. Removing pathology from an image is a research problem in itself, but commonly a registration approach with a healthy brain - often an atlas - is used [5,18,14]. We propose to not use an atlas but rather the contralateral side of the brain as a reference for healthy brain structure (similar to [6]). Using a registration of the T1-weighted image with its left-right mirrored version, all segmentations were transferred to the contralateral healthy side of the brain. To prevent unrealistic warping of the image due to image intensity changes in the tumor, while still capturing its mass effect, the b-spline registration was regularized with a bending energy penalty [16]. The weight of this penalty with the mutual information metric was tuned on a number of cases using visual inspection of the transformation.

The model input is a segmentation of the brain, separated into white matter ( $\mathcal{W}$ ) and gray matter ( $\mathcal{G}$ ), potentially an estimate of the local diffusion based on Diffusion Tensor Imaging (DTI), and a binary segmentation of the tumor. Segmentations of the brain and brain tissue were produced using HD-BET [13] and FSL FAST [23] respectively. For the pre-operative images, which did not include a T2W-FLAIR sequence,  $S_0$  was segmented manually. Tumor segmentations  $S_1$  and  $S_2$  for consecutive images were produced using HD-GLIO [15,12] and corrected manually where necessary. Alignment with the space of  $S_0$  was achieved with a b-spline registration, which was evaluated visually. Datasets were excluded if the registration did not produce a reasonable alignment.

As no registration or segmentation will be perfect, some inconsistencies remain that prevent a perfect prediction. To not punish the model unfairly, the voxels in  $S$  falling outside the brain were disregarded in the computation of the Average Precision metric.

### 3.4 Patient selection

A retrospective dataset was selected from Erasmus Medical Center of patients who a) were diagnosed with a low-grade glioma; b) were treated with surgical resection, but received no chemo- or radiotherapy; and c) had a DTI and 3D T1-weighted scan before resection, and two follow-up scans (before and after tumor progression). This resulted in data of 21 patients, after one dataset was

excluded due to failed registration. Note that the time difference between the measurement of initial tumor and the two follow-up scans varied from a few months to several years.

### 3.5 Parameters

As the variation of diffusive behavior within the brain is most defining for the tumor shape, we used  $\kappa_w$ ,  $\kappa_g$  and  $\tau$  as parameters of interest, while keeping the proliferation constant at  $\rho = 0.01$ . These parameters were not fitted but rather varied systematically, as listed with the results in 3. For this range of seven growth model parameter settings, the AP performance was measured for goodness-of-fit on the baseline segmentation  $S_0$  and predictive performance on  $S_2$ , according to the two evaluation schemes. The relation between goodness-of-fit and predictive performance was quantified using a patient-wise Spearman correlation across different growth model parameter settings. The mean of the patient-wise correlation coefficients was tested for a significant difference from zero using a one-sample t-test.

## 4 Results

Figure 3 shows a comparison of the goodness-of-fit, which is measured by the average precision on the initial tumor segmentation  $S_0$  and the final predictive performance on  $S_2$ .

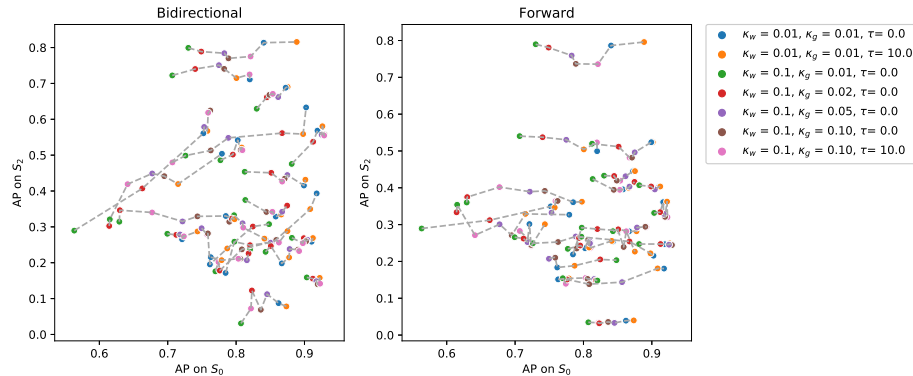


**Fig. 3.** Comparison of goodness-of-fit versus predictive performance for the two evaluation setups. Results for the same patient on different parameter sets are interconnected.

Comparing the performance between different growth model parameter settings, it is clear that goodness-of-fit is generally higher and more dependent on the model parameters than the predictive performance. From the growth model

parameter settings, typically the best goodness-of-fit (AP on  $S_0$ ) was achieved with low diffusion ( $\kappa_w = 0.01$ ) while the worst fit was achieved when the difference in  $\kappa$  between white and gray matter was large ( $\kappa_w = 0.1$ ,  $\kappa_g = 0.01$  or  $\kappa_g = 0.02$ ).

From the results of the bidirectional evaluation scheme, going from an initial point through  $S_0$  to  $S_2$ , it seems that there is a relation between the goodness-of-fit and the predictive performance. However, this relation disappears when using the forward evaluation scheme. These observations are confirmed by the mean patient-wise correlation coefficients, which were 0.24 (p=0.06) for the forward scheme and -0.03 (p=0.76) for the bidirectional scheme.

## 5 Discussion

This work presents a framing of the tumor growth predictions as a forward ranking problem, and describes the Average Precision metric for its evaluation. By formulating the problem in this way we can evaluate the full spatiotemporal results of the results, even if the observations are only snapshots in the form of a segmentation. A further advantage is found in the direct link to local growth speed and quantification of the local model agreement. Though these advantages are only of a qualitative nature, and do not provide a direct benefit to the model itself, we believe it to be a useful step towards the improvement and better comparison of tumor growth predictions. An important underlying assumption in this framework is that the time axis is not quantified, so the prediction does not provide information on the overall speed of growth or any potential mass effect. Predicting the growth speed is a highly relevant problem as well, but very different in nature from the spatial distribution.

The importance of framing the problem is further illustrated with the experimental setup. Specifically for personalized tumor growth models, which are fitted to an initial tumor shape, this work presents a forward scheme that separates the goodness-of-fit from the evaluation of future predictions. Using this scheme, and comparing to a bidirectional alternative, we show that the goodness-of-fit and predictive performance are not necessarily correlated. However, we should be careful in interpreting these results as the underlying reason for the disparity is unclear. If the goal is to find the model that best fits the available data, this strict separation might not be useful.

When moving towards statistical models for tumor growth, the framing of the problem is essential. Between the actual mechanisms of tumor growth and the segmentation is a flawed observation on MR imaging, the rather difficult problem of segmentation and registration and an estimate of the time horizon. Those factors, combined with limited data and the fact that glioma are naturally unpredictable are a major reason why tumor growth models have relied heavily on simulations [9] and qualitative observations [2] for their validation. This work is a step towards the comparison and clinical evaluation of tumor growth predictions that fits their spatiotemporal nature, and allows for localized interpretation.



## Acknowledgements

This work was supported by the Dutch Cancer Society (project number 11026, GLASS-NL) and the Dutch Organization for Scientific Research (NWO).

## References

1. Alnaes, M.S., Blechta, J., Hake, J., Johansson, A., Kehlet, B., Logg, A., Richardson, C., Ring, J., Rognes, M.E., Wells, G.N.: The FEniCS Project Version 1.5 **3**(100), 9–23 (2015)
2. Angeli, S., Emblem, K.E., Due-Tønnessen, P., Stylianopoulos, T.: Towards patient-specific modeling of brain tumor growth and formation of secondary nodes guided by DTI-MRI. *NeuroImage: Clinical* **20**, 664–673 (2018)
3. Angelini, E., Clatz, O., Mandonnet, E., Konukoglu, E., Capelle, L., Duffau, H.: Glioma Dynamics and Computational Models: A Review of Segmentation, Registration, and In Silico Growth Algorithms and their Clinical Applications. *Current Medical Imaging Reviews* **3**(4), 262–276 (2007)
4. Bakas, S., Reyes, M., Jakab, A., Bauer, S., Rempfler, M., Crimi, A., ..., Menze, B.: Identifying the best machine learning algorithms for brain tumor segmentation, progression assessment, and overall survival prediction in the BRATS challenge. *arXiv* **124** (2018)
5. Bakas, S., Zeng, K., Sotiras, A., Rathore, S., Akbari, H., Gaonkar, B., Rozycki, M., Pati, S., Davatzikos, C.: GLISTRboost: Combining multimodal MRI segmentation, registration, and biophysical tumor growth modeling with gradient boosting machines for glioma segmentation. vol. 9556, pp. 144–155 (2016)
6. Clatz, O., Sermesant, M., Bondiau, P.Y., Delingette, H., Warfield, S.K., Malandain, G., Ayache, N.: Realistic simulation of the 3-D growth of brain tumors in MR images coupling diffusion with biomechanical deformation. *IEEE Transactions on Medical Imaging* **24**(10), 1334–1346 (2005)
7. Elazab, A., Bai, H., Abdulazeem, Y.M., Abdelhamid, T., Zhou, S., Wong, K.K., Hu, Q.: Post-Surgery Glioma Growth Modeling from Magnetic Resonance Images for Patients with Treatment. *Scientific Reports* **7**(1) (2017)
8. Elazab, A., Wang, C., Gardezi, S.J.S., Bai, H., Hu, Q., Wang, T., Chang, C., Lei, B.: GP-GAN: Brain tumor growth prediction using stacked 3D generative adversarial networks from longitudinal MR Images. *Neural Networks* **132**, 321–332 (2020)
9. Ezhov, I., Lipkova, J., Shit, S., Kofler, F., Collomb, N., Lemasson, B., Barbier, E., Menze, B.: Neural Parameters Estimation for Brain Tumor Growth Modeling. In: *MICCAI 2019*, pp. 787–795 (2019)
10. Gaw, N., Hawkins-Daarud, A., Hu, L.S., Yoon, H., Wang, L., Xu, Y., Jackson, P.R., Singleton, K.W., Baxter, L.C., Eschbacher, J., Gonzales, A., Nespodzany, A., Smith, K., Nakaji, P., Mitchell, J.R., Wu, T., Swanson, K.R., Li, J.: Integration of machine learning and mechanistic models accurately predicts variation in cell density of glioblastoma using multiparametric MRI. *Scientific Reports* **9**(1), 1–9 (2019)
11. Gholami, A., Mang, A., Biro, G.: Mathematical Biology An inverse problem formulation for parameter estimation of a reaction-diffusion model of low grade gliomas. *J. Math. Biol* **72**, 409–433 (2016)
12. Isensee, F., Jaeger, P.F., Kohl, S.A., Petersen, J., Maier-Hein, K.H.: nnU-Net: a self-configuring method for deep learning-based biomedical image segmentation. *Nature Methods* (2020)

13. Isensee, F., Schell, M., Pflueger, I., Brugnara, G., Bonekamp, D., Neuberger, U., Wick, A., Schlemmer, H., Heiland, S., Wick, W., Bendszus, M., Maier-Hein, K.H., Kickingereder, P.: Automated brain extraction of multisequence MRI using artificial neural networks. *Human Brain Mapping* **40**(17), 4952–4964 (2019)
14. Jacobs, J., Rockne, R.C., Hawkins-Daarud, A.J., Jackson, P.R., Johnston, S.K., Kinahan, P., Swanson, K.R.: Improved model prediction of glioma growth utilizing tissue-specific boundary effects. *Mathematical Biosciences* **312**, 59–66 (2019)
15. Kickingereder, P., Isensee, F., Tursunova, I., Petersen, J., Neuberger, U., Bonekamp, D., Brugnara, G., Schell, M., Kessler, T., Foltyn, M., Harting, I., Sahm, F., Prager, M., Nowosielski, M., Wick, A., Nolden, M., Radbruch, A., Debus, J., Schlemmer, H.P., Heiland, S., Platten, M., von Deimling, A., van den Bent, M.J., Gorlia, T., Wick, W., Bendszus, M., Maier-Hein, K.H.: Automated quantitative tumour response assessment of MRI in neuro-oncology with artificial neural networks: a multicentre, retrospective study. *The Lancet Oncology* **20**(5), 728–740 (2019)
16. Klein, S., Staring, M., Murphy, K., Viergever, M.A., Pluim, J.P.: Elastix: A toolbox for intensity-based medical image registration. *IEEE Transactions on Medical Imaging* **29**(1), 196–205 (2010)
17. Konukoglu, E., Clatz, O., Menze, B.H., Stieltjes, B., Weber, M.A., Mandonnet, E., Delingette, H., Ayache, N.: Image guided personalization of reaction-diffusion type tumor growth models using modified anisotropic eikonal equations. *IEEE Transactions on Medical Imaging* **29**(1), 77–95 (2010)
18. Lipkova, J., Angelikopoulos, P., Wu, S., Alberts, E., Wiestler, B., Diehl, C., Preibisch, C., Pyka, T., Combs, S.E., Hadjidooukas, P., Van Leemput, K., Kourmoutsakos, P., Lowengrub, J., Menze, B.: Personalized Radiotherapy Design for Glioblastoma: Integrating Mathematical Tumor Models, Multimodal Scans, and Bayesian Inference. *IEEE Transactions on Medical Imaging* **38**(8), 1875–1884 (2019)
19. Petersen, J., Jäger, P.F., Isensee, F., Kohl, S.A.A., Neuberger, U., Wick, W., Debus, J., Heiland, S., Bendszus, M., Kickingereder, P., Maier-Hein, K.H.: Deep probabilistic modeling of glioma growth. In: *Proc. MICCAI*. pp. 806–814 (2019)
20. Powell, M.J.D.: The BOBYQA algorithm for bound constrained optimization without derivatives. Tech. rep. (2009)
21. Reikik, I., Allasonnière, S., Clatz, O., Geremia, E., Stretton, E., Delingette, H., Ayache, N.: Tumor growth parameters estimation and source localization from a unique time point: Application to low-grade gliomas. *Computer Vision and Image Understanding* **117**(3), 238–249 (2013)
22. Silbergeld, D.L., Chicoine, M.R.: Isolation and characterization of human malignant glioma cells from histologically normal brain. *Journal of Neurosurgery* **86**(3), 525–531 (1997)
23. Zhang, Y., Brady, M., Smith, S.: Segmentation of brain MR images through a hidden Markov random field model and the expectation-maximization algorithm. *IEEE Transactions on Medical Imaging* **20**(1), 45–57 (2001)